

Scalable, Tunable Josephson Junctions and DC SQUIDS Based on CVD Graphene

Tianyi Li , John C. Gallop, Ling Hao , and Edward J. Romans

Abstract—Since the carrier density and resistivity of graphene are heavily dependent on the Fermi level, Josephson junctions with graphene as the weak link can have their I - V properties easily tuned by the gate voltage. Most of the previous work on superconductor-graphene-superconductor (SGS) junctions and superconducting quantum interference devices (SQUIDS) were based on mechanically exfoliated graphene, which is not compatible with large scale production. Here, we show that SGS junctions and dc SQUIDS can be easily fabricated from chemical vapor deposition (CVD) graphene and exhibit good electronic properties. The SGS junctions can work without any hysteresis in their electrical characteristics from 1.5 K down to a base temperature of 320 mK, and the critical current can be effectively tuned by the gate voltage by up to an order of magnitude. As a result, dc SQUIDS made up of these junctions can have their critical current tuned by both the magnetic field and the gate voltage.

Index Terms—Josephson junctions, nanomaterials, SQUIDS, superconducting devices.

I. INTRODUCTION

DUE to their unique non-linear inductance, Josephson junctions or dc superconducting quantum interference devices (SQUIDS) have become the building blocks and key elements of superconducting qubits, which are a promising solid-state approach to realizing quantum computing [1]–[3]. When scaling up designs from more than one superconducting qubit, some of the qubits and their coupling resonators are required to have exactly the same energy-level spacing in order to achieve high-fidelity multi-qubit gates. However, due to limitations in fabrication techniques, it is almost impossible to make perfectly identical Josephson junctions based on conventional sandwich structures. Such a problem is normally solved by replacing a single Josephson junction with a dc SQUID and accompanying it with a nearby current-carrying control line. As a result,

Manuscript received October 28, 2018; accepted February 1, 2019. Date of publication February 7, 2019; date of current version March 18, 2019. This work was supported in part by the U.K. National Measurement System, under the EU Project EMPIR 17FUN06 SIQUST, and in part by the U.K. Engineering and Physical Sciences Research Council (EPSRC) under Grant EP/M508330/1, Grant EP/J007137/1, and Grant 1437148. (Corresponding author: Tianyi Li.)

T. Li was with the University College London, London WC1E 6BT, U.K., and also with the National Physical Laboratory, Teddington TW11 0LW, U.K. He is now with Aalto University, Espoo 02150, Finland (e-mail: tianyi.li.14@ucl.ac.uk).

J. C. Gallop and L. Hao are with the National Physical Laboratory, Teddington TW11 0LW, U.K. (e-mail: john.gallop@npl.co.uk; ling.hao@npl.co.uk).

E. J. Romans is with the University College London, London WC1E 6BT, U.K. (e-mail: e.romans@ucl.ac.uk).

Color versions of one or more of the figures in this paper are available online at <http://ieeexplore.ieee.org>.

Digital Object Identifier 10.1109/TASC.2019.2897999

the critical current of the SQUID can be tuned by the local magnetic field, so that the energy-level spacing of the qubit or the resonator can also be tunable. However, as the number of qubits and the number of coupling resonators increases on a chip, the configuration of magnetic current leads can become challenging, and crosstalk between magnetic fields will become a significant source of error [4]. Therefore, Josephson junctions and dc SQUIDS with other degrees of freedom in their electronic properties are highly desirable.

The distinct band structure of graphene means that superconductor-graphene-superconductor (SGS) Josephson junctions have a critical current that can be gradually tuned by a local electric gate [5]. Since the first SGS junction was experimentally implemented by Heersche *et al.* in 2007 [6], graphene-based Josephson junctions and SQUIDS have become a hot topic of research in the last decade [7]–[13], and many novel phenomena including multiple Andreev reflection [8], [10], [13] and ballistic transport [9]–[12] have been discovered and discussed. Previous research on SGS junctions and SQUIDS was mostly based on mechanically exfoliated graphene, which is not compatible with large-scale synthesis and device fabrication. The fabrication and measurement of SGS junctions compatible with real applications in superconducting circuits remains largely unexplored [14], and integrating SGS junctions and SQUIDS into superconducting qubits is still some way off [15], [16]. In this work, we show that SGS junctions and dc SQUIDS based on chemical-vapor-deposition (CVD) graphene exhibit ideal electronic properties with the critical current easily tuned by the gate voltage, and can be promising candidates for applications such as superconducting qubits.

II. METHODS

We have developed a robust process to fabricate Josephson junctions based on CVD graphene, which is compatible with wafer-scale production. The CVD graphene samples used in our experiment (GrapheneaTM) were synthesized and transferred to a silicon substrate with a 300-nm-thick oxide layer. After the transfer, the graphene samples were examined by Raman spectroscopy. The laser wavelength used was 532 nm and the spot size of the laser beam was around 10 μm . As shown in Fig. 1(a), the intensity of the 2D peak ($\sim 2680\text{ cm}^{-1}$) is more than 2.5 times as that of the G peak ($\sim 1584\text{ cm}^{-1}$), indicating that the graphene is mostly mono-layer [17], [18]. The D peak ($\sim 1350\text{ cm}^{-1}$) is hardly seen in the spectrum, which means that impurities and defects are rare in the sample [19]. The inset

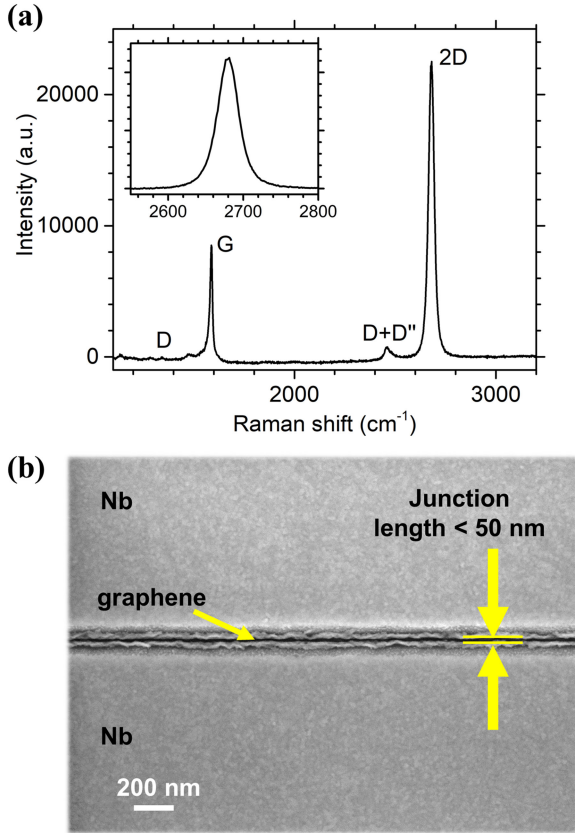


Fig. 1. (a) A Raman spectrum of a CVD synthesised graphene sample transferred to a silicon substrate with an oxide layer. The intensity of the 2D peak is more than 2.5 times that of the G peak, which is clear evidence that the graphene is mono-layer. Inset: the magnification of the spectrum near the 2D band. The shape of the 2D band clearly shows that it contains only one peak. (b) An SEM image of part of a short and wide superconductor-graphene-superconductor (SGS) junction. The graphene is covered by two Nb electrodes and only exposed to the atmosphere in the narrow gap between the electrodes, as indicated by the arrow on the left. By carefully controlled e-beam lithography and lift-off, the junction length can be shorter than 50 nm, with no leakage between the two superconducting electrodes, even for electrodes up to $80 \mu\text{m}$ wide, which extend much further horizontally than shown in the image.

of Fig. 1(a) shows the zoom-in of the spectrum around the 2D band. The 2D band only consists of a single peak, which again indicates that the graphene sample is mono-layer.

To fabricate the Josephson junctions, we used electron beam lithography (EBL) to define superconducting (Nb) electrodes on top of the graphene. After developing the e-beam resist, we sputter a tri-layer of Ti (5 nm)/ Nb (70 nm)/ Au (8 nm) onto the sample, followed by lift-off without sonication. By using double layers of poly(methyl methacrylate) (PMMA) as the e-beam resist and sputtering the tri-layer metal film at a lower rate to prevent overheating the sample, we managed to fabricate short and wide Josephson junctions in a controllable way with a very high throughput. The shortest junction can be shorter than 50 nm, as shown in the scanning electron microscope (SEM) image in Fig. 1(b). After defining the junctions, another EBL process was used to remove the graphene surrounding the devices by Ar milling, so that the devices were isolated from one another and the junctions had no additional shunt resistance outside the gap region between the electrodes. The

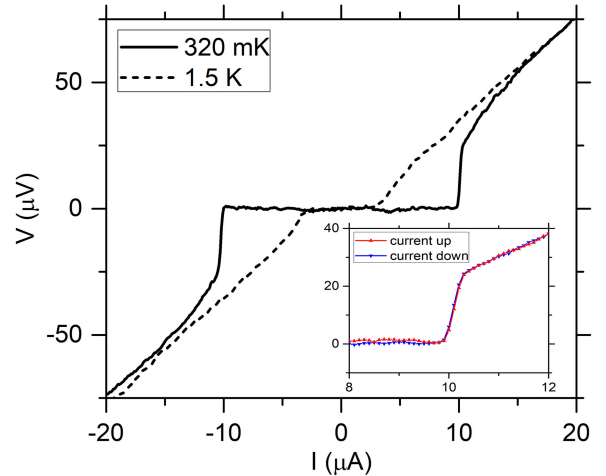


Fig. 2. I - V characteristics of an SGS junction with length $L = 250 \text{ nm}$ and width $W = 80 \mu\text{m}$, measured at 320 mK and 1.5 K respectively. The inset is a zoom-in of the transition around the critical current at 320 mK showing no hysteresis when current is swept upwards or downwards.

highly-doped silicon substrate was connected as the back gate. The average contact resistivity we obtain between graphene and the Nb electrode is around $100 \Omega \cdot \mu\text{m}$, which is amongst the lowest reported in the literature for graphene/metal contacts [20]. The devices were then measured in a ^3He cryostat with a base temperature of 320 mK.

III. RESULTS

A. I - V Characteristics of SGS Junctions

To reduce the normal state resistance R_n and increase the critical current I_c for ease of measurement, the SGS junctions we fabricated were relatively short (50~450 nm) and wide (10~80 μm). As shown in Fig. 2, the measurements show that the junctions exhibit I - V characteristics at 320 mK without any hysteresis, as predicted by the resistively and capacitively shunted junction (RCSJ) model for over-damped junctions. By measuring the I - V characteristics of junctions of different length and width, we have found that the critical current and the normal state conductance show a linear dependence on the junction width. The critical current per unit width is around $0.1 \mu\text{A}/\mu\text{m}$ at 320 mK, whereas the normal state resistivity (normal state resistance times the junction width) is around $300 \Omega \cdot \mu\text{m}$. Although a higher critical current density has been reported for SGS junctions based on mechanically exfoliated graphene and Pb/Pd electrodes [21], our junctions have the advantage of being free of hysteresis which makes them especially suitable for use in dc SQUIDS with conventional readout. For our junctions we also notice that the critical current and the normal state resistance don't show a clear dependence on the junction length, which suggests that the normal state resistance is dominated by the contact resistance between graphene and the superconducting electrode. As temperature gradually increases, the critical current I_c decreases and the current-voltage transition close to I_c becomes slightly rounded due to thermal noise. The Josephson effect is still obvious up to 1.5 K as shown in Fig. 2, indicating

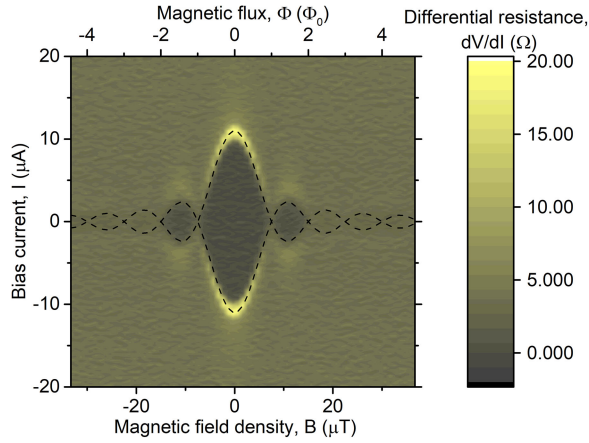


Fig. 3. Differential resistance dV/dI as a function of the bias current I and the perpendicular magnetic field density B , measured on an SGS junction with a length of 250 nm and a width of 80 μm . The central dark region is where the differential resistance is almost zero and the bright outline of the dark region refers to the transition at the critical current I_c . The critical current shows a Fraunhofer-like interference pattern under perpendicular magnetic field, which can be fitted by the black dashed line, $I_c \propto \sin(\pi B/\Delta B)/(B/\Delta B)$. The top axis is determined by the expected periodicity of the minima in the Fraunhofer-like pattern. The ratio of the top axis and the bottom axis is equal to the effective area of the junction, which is 280 μm^2 .

that such junctions can operate over a usefully wide temperature range.

Under a perpendicular magnetic field, the SGS junctions show the effect of self-interference as the junctions are of finite area. In Fig. 3, we plot the differential resistance dV/dI as a function of the bias current I and the magnetic field density B in a contour plot. The dark region in the center is zero-resistance regime and the bright outline of the dark region refers to the transition at the critical current I_c . The $I_c - B$ relation shows an ideal Fraunhofer-like pattern, with higher order peaks clearly visible, indicating that the junction is still quite uniform in terms of the distribution of its supercurrent density, even for SGS junctions as wide as 80 μm . The theory of Josephson junctions shows that the supercurrent distribution is uniform only when the junction width is relatively small compared with the Josephson penetration depth λ_J [22]. The standard expression for the Josephson penetration depth of a conventional tunnel junction is

$$\lambda_J = \sqrt{\frac{\Phi_0}{2\pi\mu_0 j_c (t + 2\lambda_L)}}, \quad (1)$$

where $\Phi_0 = h/2e$ is the quantum flux, j_c is the critical current density (critical current per unit area), t is the geometric barrier thickness of the junction, and λ_L is the London penetration depth of the superconducting electrodes. The Josephson penetration depth calculated by (1) for SGS junctions is only 2.5 μm , which is much smaller than the junction width. The fact that we managed to observe uniform distribution of supercurrent in the wide SGS junctions suggests that the expression of Josephson penetration depth in (1) needs altering for coplanar junctions based on 2-dimensional materials. A similar phenomenon has been observed in coplanar Josephson junctions based on high- T_c superconductors [23].

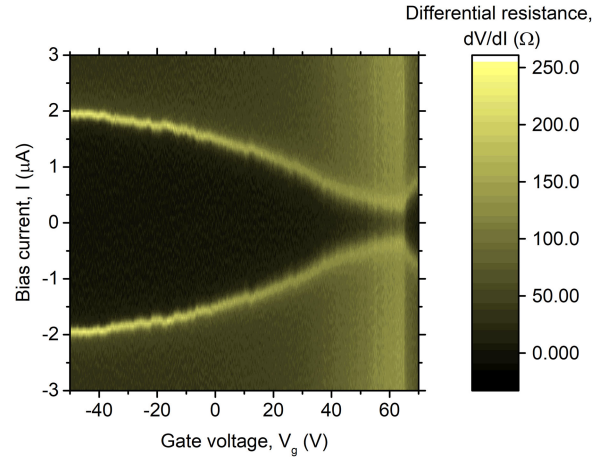


Fig. 4. Differential resistance dV/dI as a function of the bias current I and the gate voltage V_g , measured on an SGS junction with a length of 50 nm and a width of 10 μm . The central dark region is where the differential resistance is almost zero and the bright outline of the dark region refers to the transition at the critical current I_c . The critical current reaches its minimum at the Dirac point when $V_g = 64$ V, and shows a bipolar increase on both sides of the Dirac point. The normal state resistance is also modulated from 40 Ω to 160 Ω as the gate voltage changes from -50 V to the Dirac point.

Fig. 4 shows how the $I-V$ properties of a Josephson junction can be tuned by the gate voltage. The differential resistance dV/dI is plotted versus bias current I and gate voltage V_g in a 2D contour plot. The dark region in the center is the zero-resistance regime and the bright outline of the dark region indicates the transition at the critical current I_c . As the gate voltage increases from -50 V to $+70$ V, the critical current gradually decreases from 1.9 μA , reaches the minimum of 0.2 μA at the Dirac point (where $V_g \equiv V_0 = 63.85$ V), and then starts to increase. The tuning range of critical current by the gate voltage is as large as an order of magnitude, so that the Josephson energy of the junction $E_J = \Phi_0 I_c / 2\pi$ can be similarly tuned by an order of magnitude. Thus, the energy-level spacing of superconducting qubits or resonators built by the SGS junctions can be tuned by the local electric gate up to a similar range, which is probably large enough for most applications.

To further characterize the properties of the graphene in the SGS junctions, we have fabricated some Hall bar structures on the same CVD graphene sample, using the same fabrication techniques as for the junctions. The width of the Hall bar is 10 μm . By a combination of 4-probe measurement and Hall measurement at low temperature, we can find that the sheet resistance of the graphene is 460 Ω/\square , the area carrier density is $5.5 \times 10^{12} \text{ cm}^{-2}$ and that the mobility of the charge carriers is 2100 cm^2/Vs . The mean free path is then derived to be about 60 nm, which is relatively high among exposed CVD graphene samples, but much lower than the mean free path of CVD graphene encapsulated in hexagonal boron nitride [24]. As the mean free path in graphene is comparable to the length of the shortest junction (50 nm), the critical current is expected to show oscillation as a function of gate voltage in Fig. 4, which is a signature of ballistic transport [12]. However, the oscillation of critical current in Fig. 4 is hard to distinguish and not convincing enough, which we think is because i) the junction

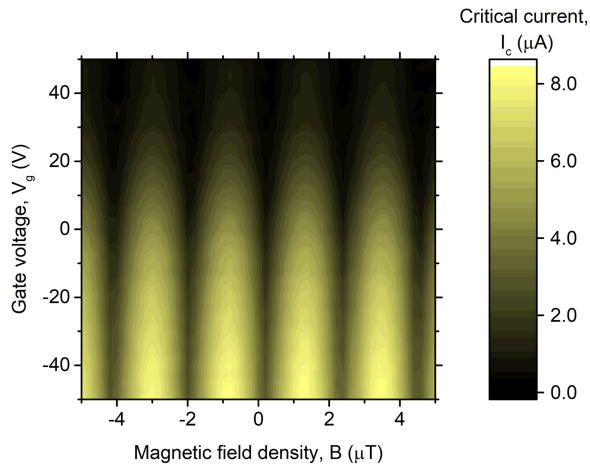


Fig. 5. Critical current I_c as a function of the magnetic field density B and the gate voltage V_g , measured on an SGS dc SQUIDs with an inner loop size of $500 \mu\text{m}^2$. The lengths of the two junctions are 50 nm and the widths are $20 \mu\text{m}$. The critical current can be tuned periodically by the perpendicular magnetic field and monotonically by the gate voltage.

length is not much smaller than the mean free path so that the signature of ballistic transport is not strong enough, and ii) the accuracy of measuring the critical current is limited by the noise level in our system.

B. I-V Characteristics of DC SQUIDs

We have also utilized similar techniques to fabricate dc SQUIDs based on the SGS junctions, with an inner loop area of $500 \mu\text{m}^2$ and an outer loop area of $1500 \mu\text{m}^2$. The two SGS junctions in parallel each have a length of 50 nm and a width of $20 \mu\text{m}$. Under a perpendicular magnetic field, the critical current of the SQUIDs shows high frequency oscillation, which can be seen if we make a horizontal cross section of Fig. 5. At larger fields than shown, the high frequency oscillation becomes modulated by the single junction response. The high frequency oscillation shown corresponds to an effective area of $910 \mu\text{m}^2$, which lies between the inner loop area and the outer loop area of the SQUID as might be expected due to the effect of flux focusing.

If we further tune the gate voltage, we can see the critical current behaves as a function of both the magnetic field and the gate voltage, as shown in Fig. 5. The critical current can be tuned periodically by the perpendicular magnetic field and monotonically by the gate voltage. The modulation depth by the gate voltage is even higher than the modulation depth by the magnetic field. The two-dimensional modulation of the critical current allows for more flexibility in operating the SQUIDs compared to conventional devices.

IV. CONCLUSION

We have developed a method to fabricate scalable and tunable Josephson junctions and dc SQUIDs based on CVD graphene. The devices can work over a wide temperature range without hysteresis, and the critical current can be effectively tuned by the gate voltage. Such tunable and scalable SGS junctions are especially useful for application involving arrays of Josephson

junctions, such as superconducting qubits and single flux quantum (SFQ) devices, where the properties of the junctions can be tuned to be identical by an electric gate.

ACKNOWLEDGMENT

The authors would like to thank A. Zurutuza at GrapheneaTM for the graphene samples, and J. Fenton and P. Warburton for help with the low-temperature system.

REFERENCES

- [1] J. Clarke and F. K. Wilhelm, "Superconducting quantum bits," *Nature*, vol. 453, no. 7198, pp. 1031–1042, Jun. 2008.
- [2] M. H. Devoret, A. Wallraff, and J. M. Martinis, "Superconducting qubits: A short review," arXiv:0411174 [cond-mat], Nov. 2004.
- [3] G. Wendin, "Quantum information processing with superconducting circuits: a review," *Rep. Prog. Phys.*, vol. 80, no. 10, Sep. 2017, Art. no. 106001.
- [4] D. Rosenberg *et al.*, "3-D integrated superconducting qubits," *NPJ Quantum Inf.*, vol. 3, no. 1, Sep. 2017, Art. no. 42.
- [5] M. Titov and C. W. J. Beenakker, "Josephson effect in ballistic graphene," *Phys. Rev. B*, vol. 74, no. 4, Jul. 2006, Art. no. 041401.
- [6] H. B. Heersche, P. Jarillo-Herrero, J. B. Oostinga, L. M. K. Vandersypen, and A. F. Morpurgo, "Bipolar supercurrent in graphene," *Nature*, vol. 446, no. 7131, pp. 56–59, Mar. 2007.
- [7] C. Girit *et al.*, "Tunable graphene dc superconducting quantum interference device," *Nano Lett.*, vol. 9, no. 1, pp. 198–199, Nov. 2009.
- [8] X. Du, I. Skachko, and E. Y. Andrei, "Josephson current and multiple Andreev reflections in graphene SNS junctions," *Phys. Rev. B*, vol. 77, no. 18, May 2008, Art. no. 184507.
- [9] V. E. Calado *et al.*, "Ballistic Josephson junctions in edge-contacted graphene," *Nat. Nanotechnol.*, vol. 10, no. 9, pp. 761–764, Jul. 2015.
- [10] I. V. Borzenets *et al.*, "Ballistic graphene Josephson junctions from the short to the long junction regimes," *Phys. Rev. Lett.*, vol. 117, no. 23, Dec. 2016, Art. no. 237002.
- [11] N. Mizuno, B. Nielsen, and X. Du, "Ballistic-like supercurrent in suspended graphene Josephson weak links," *Nat. Commun.*, vol. 4, Nov. 2013, Art. no. 2716.
- [12] M. Ben Shalom *et al.*, "Quantum oscillations of the critical current and high-field superconducting proximity in ballistic graphene," *Nat. Phys.*, vol. 12, no. 4, pp. 318–322, Apr. 2016.
- [13] C. Li, S. Guéron, A. Chepelianskii, and H. Bouchiat, "Full range of proximity effect probed with superconductor/graphene/superconductor junctions," *Phys. Rev. B*, vol. 94, no. 11, Sep. 2016, Art. no. 115405.
- [14] C. T. Ke *et al.*, "Critical current scaling in long diffusive graphene-based Josephson junctions," *Nano Lett.*, vol. 16, no. 8, pp. 4788–4791, Jul. 2016.
- [15] J. G. Kroll *et al.*, "Magnetic field compatible circuit quantum electrodynamics with graphene Josephson junctions," *Nat. Commun.*, vol. 9, Nov. 2018, Art. no. 4615.
- [16] F. E. Schmidt, M. D. Jenkins, K. Watanabe, T. Taniguchi, and G. A. Steele, "A ballistic graphene superconducting microwave circuit," *Nat. Commun.*, vol. 9, no. 1, Oct. 2018, Art. no. 4069.
- [17] A. C. Ferrari and D. M. Basko, "Raman spectroscopy as a versatile tool for studying the properties of graphene," *Nat. Nanotechnol.*, vol. 8, no. 4, pp. 235–246, Apr. 2013.
- [18] A. C. Ferrari *et al.*, "Raman spectrum of graphene and graphene layers," *Phys. Rev. Lett.*, vol. 97, no. 18, Nov. 2006, Art. no. 187401.
- [19] A. C. Ferrari and J. Robertson, "Resonant Raman spectroscopy of disordered, amorphous, and diamondlike carbon," *Phys. Rev. B*, vol. 64, no. 7, Jul. 2001, Art. no. 075414.
- [20] F. Xia, V. Perebeinos, Y. Lin, Y. Wu, and P. Avouris, "The origins and limits of metal-graphene junction resistance," *Nat. Nanotechnol.*, vol. 6, no. 3, pp. 179–184, Feb. 2011.
- [21] U. C. Coskun, M. Brenner, T. Hymel, V. Vakaryuk, A. Levchenko, and A. Bezryadin, "Distribution of supercurrent switching in graphene under the proximity effect," *Phys. Rev. Lett.*, vol. 108, no. 9, 2012, Art. no. 097003.
- [22] J. Clarke and A. I. Braginski, *The SQUID Handbook*. Weinheim, Germany: Wiley, 2006.
- [23] S. K. Tolpygo, M. Gurvitch, S. K. Tolpygo, and M. Gurvitch, "Critical currents and Josephson penetration depth in planar thin-film high-Tc Josephson junctions," vol. 69, no. 25, pp. 3914–3916, Oct. 1996.
- [24] L. Banszerus *et al.*, "Ballistic transport exceeding $28 \mu\text{m}$ in CVD grown graphene," *Nano Lett.*, vol. 16, no. 2, pp. 1387–1391, 2016.